THE ASTROPHYSICAL JOURNAL, 428:143–156, 1994 June 10

THE *HUBBLE SPACE TELESCOPE* EXTRAGALACTIC DISTANCE SCALE KEY PROJECT.[1] II. PHOTOMETRY OF WFC IMAGES OF M81[2]

SHAUN M. G. HUGHES
Palomar Observatory, 105-24, California Institute of Technology, Pasadena, CA 91125;
I: smh@phobos.caltech.edu

PETER B. STETSON
National Research Council, Dominion Astrophysical Observatory, 5071 W. Saanich Rd., Victoria, BC, Canada V8X 4M6;
I: stetson@dao.nrc.ca

ANNE TURNER AND ROBERT C. KENNICUTT, JR.
Steward Observatory, University of Arizona, Tucson, AZ 85721;
I: aturner@as.arizona.edu, robk@as.arizona.edu

ROBERT HILL, MYUNG GYOON LEE,[3] AND WENDY L. FREEDMAN[4]
Carnegie Observatories, 813 Santa Barbara St., Pasadena, CA 91101;
I: hill@ociw.edu, mglee@ociw.edu, wendy@ociw.edu

JEREMY R. MOULD AND BARRY F. MADORE[4]
California Institute of Technology, Pasadena, CA 91125;
I: barry@ipac.caltech.edu, jrm@deimos.caltech.edu

LAURA FERRARESE AND HOLLAND C. FORD
Space Telescope Science Institute, Homewood Campus, Baltimore, MD 21218;
I: ferrarese@scivax.stsci.edu, ford@scivax.stsci.edu

JOHN A. GRAHAM
Department of Terresterial Magnetism, Carnegie Institution of Washington, 5241 Broad Branch Rd. N.W., Washington, DC 20015;
I: graham@jag.ciw.edu

JOHN G. HOESSEL
Department of Astronomy, University of Wisconsin, 475 N. Charter St., Madison, WI 53706;
hoessel@uwfpc.span

AND

GARTH D. ILLINGWORTH
Lick Observatory, University of California, Santa Cruz, CA 95064;
I: gdi@helios.ucsc.edu

Received 1993 December 1; accepted 1993 December 2

ABSTRACT

The Extragalactic Distance Scale (H_0) Key Project for *Hubble Space Telescope* (*HST*) aims to employ the Cepheid period-luminosity ($P-L$) relation to measure galaxy distances out as far as the Virgo Cluster. The vital steps in this program are (1) to obtain precise photometry of stellar images from the Wide Field Camera (WFC) exposures of selected galaxies, and (2) to calibrate this photometry to obtain reliable distances to these galaxies from the Cepheid $P-L$ relation. We have used the DAOPHOT II and ALLFRAME programs to determine 28 instrumental magnitudes—22 of F555W ($\sim V$) and six of F785LP ($\sim I$)—of all stars brighter than $V \sim 25$ in each of two 2'.56 × 2'.56 WFC fields of M81. The reductions use a varying point-spread function to account for the field effects in the WFC optics and yield instrumental magnitudes with single epoch precision ranging from 0.09 to 0.24 mag, at $V \sim 21.8$ to 23.8—the magnitude range of the 30 Cepheids that we have now identified in M81. For brighter stars ($V < 22$), single epoch magnitudes are precise to 0.09 mag. The photometric calibration onto the Johnson V and Kron-Cousins I systems was determined from independent ground-based CCD observing at the CFHT 3.6 m (confirmed by the KPNO 4.0 m) and from the Palomar 5.0 m (using the wide-field COSMIC camera) and 1.5 m telescopes. Secondary standards, taken from the COSMIC and CFHT frames, were established in each of the WFC fields in V and I, allowing a direct transformation from ALLFRAME magnitudes to calibrated V and I magnitudes, giving mean $V \sim 23$ magnitudes accurate to $\sim \pm 0.1$ mag. The stellar populations in M81 have been analyzed in terms of the luminosity functions and color magnitude diagrams (CMD) derived from these data, from which we identify numerous supergiants, and a CMD morphology similar to M33.

Subject headings: Cepheids — galaxies: individual (M81) — galaxies: photometry — stars: luminosity function, mass function

[1] Based on observations with the NASA/ESA *Hubble Space Telescope*, obtained at the Space Telescope Science Institute, which is operated by the Association of Universities for Research in Astronomy, Inc., under NASA contract NAS 5-26555.

[2] Based in part on observations made at Palomar Observatory, which is owned and operated by the California Institute of Technology (Caltech). The Palomar 1.5 m telescope is jointly owned by Caltech and the Carnegie Observatories.

[3] Current address: Department of Astronomy, Seoul National University, Korea. I: mglee@astrog.snu.ac.kr.

[4] Visiting Astronomer at the Canada-France-Hawaii Telescope, which is operated by NRC Canada. CNRS France, and the University of Hawaii.

1. INTRODUCTION

There now exist several precise methods for measuring relative distances to galaxies (e.g., surface brightness fluctuations; the IR Tully-Fisher relation for spirals; planetary nebule luminosity functions; luminosities of Type Ia supernovae), but there are still large uncertainties in the zero points for each of these secondary distance indicators. The goal of the *HST* Extragalactic Distance Scale Key Project is to use a reliable primary distance indicator, the Cepheid period-luminosity relation, to measure accurate distances to a variety of galaxies out to the Virgo Cluster, and from these distances establish the zero-point calibrations for the secondary distance indicators (Mould et al. 1993). These calibrated secondary distance indicators should then be capable of measuring Hubble's expansion parameter (H_0) to an accuracy of $\pm 10\%$.

As a first step in the project, multiepoch observations were obtained for two fields in the nearby galaxy M81, one of the few galaxies in the Key Project which is near enough to be reached with *HST*'s aberrated optics. These preliminary observations served two important purposes. The first was to detect Cepheid variables in M81 and determine an accurate distance to the galaxy, which is an important calibrator for several distance indicators. These results, derived from the detection of 30 Cepheid variables, are presented in Freedman et al. (1994, hereafter Paper I). The second objective of the M81 observations was to develop and test appropriate photometry routines that could cope with undersampled images with high cosmic-ray counts, detect variables and determine their periods from the sparsely sampled multiepoch data, and accurately calibrate the photometric scale of the aberrated Wide Field Camera (WFC) images. The latter is a particularly challenging problem, which is relevant to a wide range of scientific programs using the WFC, and is the main subject of this paper.

Calibration of WFC photometry onto a standard system is by no means straightforward. Several problems unique to the instrument are summarized in Faber & Westphal (1991; hereafter the IDT Report) and Holtzman et al. (1991). The spherical aberration causes variations in the shape of the point-spread function (PSF) across each chip, which includes changes in the ratio of the PSF's core to halo luminosity. Other problems are introduced by the flat-field calibrations of the WFC, which were obtained from streaked observations of the Earth, and show deviations from flatness of up to 20% (Phillips et al. 1993). In addition, contamination of the WFC introduces temporal variations in sensitivity of up to 15% in the bandpasses of interest (Ritchie & MacKenty 1993; Labhardt, Schwengeler, & Tammann 1993). With these complications in mind, it was clear that deriving a single internal photometric calibration for the WFC frames would lead to unacceptably large errors in the stellar photometry, and instead we chose to establish a set of secondary standards in each of the WFC M81 fields, obtained from ground-based photometry of the brighter stars, and used these to calibrate the WFC data.

In this paper we describe the calibration of the WFC photometry, and apply it to discuss the properties of the $\sim$30,000 stars detected in the two M81 fields. The paper is organized as follows. In § 2 we briefly summarize the WFC observations and the steps that were taken to process these data prior to calibration. The ground-based observations used to set up the secondary standards are described in § 3, and the calibration process itself is described in § 4. In § 5 we discuss the precision of the stellar photometry of the two fields and analyze the luminosity functions and color-magnitude diagrams of the stellar population. Our conclusions are summarized in § 6.

2. *HST* WFC PHOTOMETRY

Two fields in M81 were observed. One field contained V30, one of only two Cepheids known from ground-based observations (Freedman & Madore 1988), and the other field was chosen to sample the major axis of M81, $\sim$5.5 from the nucleus. As a compromise between Cepheid pulsation amplitude (which decreases with increasing wavelength) and mean magnitude accuracy (which improves with increasing wavelength, due to the reduced amplitude, as well as reduced extinction uncertainties), 22 WFC exposures of each field were made using the F555W filter, which covers a similar bandpass to the Johnson *V* filter. An additional six exposures were made using the F785LP filter (similar to Kron-Cousins *I*) in order to establish a mean reddening for the Cepheids (e.g., Freedman et al. 1992). A journal of observations is given in Table 1 (the modified Julian date given is for the start of each V30 field exposure, with exposure times for the major axis and V30 fields being identical at each epoch, and the major axis exposures being taken immediately prior to each of the V30 field exposures). The *HST* frames were passed through STScI's Routine Science Data Processing calibration pipeline (Lauer 1989), which makes a correction for the analog to digital conversion, subtracts bias and dark frames, and divides by flat fields. For the F555W frames, a better Earth-streak derived flat field was obtained in early 1992, and so all frames acquired prior to this were reprocessed through the pipeline. Although contamination effects (called measles) have been reported in

TABLE 1

HST WFC OBSERVATIONS OF M81

Date	MJD[a]	Exp	*HST* maj & V30 rootnames	
		— F555W exposures —		
1991 Dec 30	48620.867	900	W0TP0101T	W0TP0J01T
1991 Dec 30	48620.879	900	W0TP0102T	W0TP0J02T
1991 Dec 31	48621.803	1200	W0TP0201T	W0TP0K01T
1992 Jan 9	48630.759	1200	W0TP0301T	W0TP0L01T
1992 Jan 20	48641.150	1200	W0TP0401T	W0TP0M01T
1992 Jan 21	48642.025	1200	W0TP0501T	W0TP0N01T
1992 Jan 22	48643.098	1200	W0TP0601T	W0TP0O01T
1992 Jan 23	48644.633	1200	W0TP0701T	W0TP0P01T
1992 Jan 25	48646.231	900	W0TP0801T	W0TP0Q01T
1992 Jan 25	48646.243	900	W0TP0802T	W0TP0Q02T
1992 Jan 28	48649.062	1200	W0TP0901T	W0TP0R01T
1992 Feb 1	48653.002	900	W0TP0A01T	W0TP0S01T
1992 Feb 1	48653.014	900	W0TP0A02T	W0TP0S02T
1992 Feb 6	48658.106	1200	W0TP0B01T	W0TP0T01T
1992 Feb 11	48663.053	900	W0TP0C01T	W0TP0U01T
1992 Feb 11	48663.065	900	W0TP0C02T	W0TP0U02T
1992 Dec 28	48984.101	1200	W0TP0D01T	W0TP0V01T
1992 Dec 31	48987.380	1200	W0TP0E01T	W0TP0W01T
1993 Jan 5	48992.334	1200	W0TP0F01T	W0TP0X01T
1993 Jan 13	49000.162	1200	W0TP0G01T	W0TP0Y01T
1993 Jan 25	49012.273	1200	W0TP0H01T	W0TP0Z01T
1993 Feb 11	49029.241	1200	W0TP0I01T	W0TP1001T
		— F785LP exposures —		
1992 Jan 9	48630.815	1800	W0TP0302T	W0TP0L02T
1992 Jan 22	48643.153	1800	W0TP0602T	W0TP0O02T
1992 Jan 28	48649.113	1800	W0TP0902T	W0TP0R02T
1992 Feb 11	48663.120	1800	W0TP0C03T	W0TP0U03T
1992 Dec 31	48987.441	1800	W0TP0E02T	W0TP0W02T
1993 Jan 13	49000.291	1800	W0TP0G02T	W0TP0Y02T

[a] MJD = modified Julian date − 2,400,000 days.

shorter wavelength images, no evidence was found for this effect in any of our F555W and F785LP frames.

Although the aberrated optics of *HST* results in 84% of each star's light being spread over a 3″ radius halo (Burrows et al. 1991), the crowding in the two M81 fields is too severe and the background "sky" (from the faint unresolved stars in M81) is too bright for the halo light to be measured with any acceptable degree of precision. Hence we are restricted to photometry based on fitting the central cores. However, these cores are undersampled, and so most photometry programs that fit conventional Gaussian-like PSFs are inappropriate. The two better known programs that have been suitably modified to handle WFC PSFs are: DAOPHOT II (Stetson 1992), which allows the use of a Lorentz function as a first approximation to the PSF, and which uses empirical look-up tables to model both the fine structure and the spatial variation of the stellar profiles; and DoPHOT 2.0 (based on Mateo & Schechter's 1989 DoPHOT program), but with its pseudo-Gaussian routine replaced by a *HST*-PSF-like routine written by A. Saha (private communication) (STScI). Although both programs give similar results at the faint magnitude level of the Cepheids in M81, DAOPHOT II gives better results at brighter magnitudes (Hughes 1992). However, we chose to use DAOPHOT II principally because Stetson has written a third-generation multiple-star, multiple-frame profile-fitting package named ALLFRAME, which uses the PSF model created by DAOPHOT II, and takes advantage of the multiepoch nature of the M81 photometry (Paper I; Stetson 1994). Briefly, ALLFRAME simultaneously fits profiles to all stars contained within an ensemble of CCD images for a given field. It takes as input a list of objects and initial coordinate transformations from a reference epoch to the others, plus epoch-to-epoch magnitude offsets (due to exposure time and sensitivity differences between epochs), and a PSF model (one for each chip/filter combination) which includes second-order variation as a function of chip coordinates. A succession of PSF fits is made to all the objects on the list in each of the epoch frames. While it does so, ALLFRAME updates the coordinate transformations, and down-weights any pixels that deviate anomalously from the fit, thereby minimizing the effects of bad pixels and cosmic rays (Stetson 1987).

A major problem with most WFC images is the large number of cosmic-ray events. For the exposure times used (900 or 1200 s in F555W, and 1800 s in F785LP), a typical cosmic-ray count is ~ 50 per 10,000 pixels (or 3.2 s^{-1} per chip, slightly higher than that found by Holtzman et al. 1991), which is comparable with the mean density of stars detected in the M81 fields, this being ~ 60 stars per 10,000 pixels. Hence each stellar image (of 3″ radius) will on average be contaminated by 14 cosmic rays. However, as we are fitting only the stellar cores (with a fitting radius of 2.5 pixels), only $\sim 10\%$ of the stellar photometry is affected by cosmic rays. To provide a robust list of stellar objects for ALLFRAME, free of cosmic-ray events, median images were created of each chip in each field, in each of the F555W and F785LP filters. The precise area covered by each exposure at each epoch is offset from every other by slight (0.3 pixels in the major axis field and 8 pixels in the F555W V30 field) and sometimes not so slight (up to 100 pixels in each coordinate in the F785LP V30 field) amounts, which were determined by identifying several isolated bright stars on each chip, and matching these in each of the epoch frames, to determine translation and rotation transformations relating the various frames' coordinate systems (which were later used by ALLFRAME). These transformations were then used to shift each frame before creating a median image. The median image was used only to generate the list of positions of real objects for ALLFRAME. The ALLFRAME photometry derived from PSF fits at each of these positions was obtained from each of the single epoch frames.

For the major axis field, the PSFs (one for each filter) used in DAOPHOT and ALLFRAME were determined from combined median images of chips 1 and 2, as this yielded enough isolated stars to derive a PSF which allowed for quadratic spatial variations in the profile (Stetson 1991, 1992). For the V30 field, the PSFs were modeled on a grid of artificial stars produced by TinyTim v2.1 (kindly provided by J. Krist, STScI) for each of the four chips, and each of the two filters. TinyTim was also used to search for variations in the PSF from epoch to epoch (due to telescope outgassing which causes slight changes in focus), but the differences were found to be marginal, so only one grid of stars was produced for each chip and filter, at a mean epoch.

After the ALLFRAME reductions were completed, we realized the differences in the empirical and TinyTim PSFs may be significant. Comparisons were made by using both PSFs in DAOPHOT/ALLSTAR reductions of a 5×5 grid of chip 2 observations of the same star (HD 151406—F0 spectral type) obtained by STScI on 1991 November 9 as part of their calibration database. Over the whole chip, the mean difference between the empirical and TT PSF magnitudes was only $+0.03$ mag, with an rms of 0.15 mag. However, there was radial structure in the differences, and the mean magnitude difference for those stars within ~ 300 pixels of the center of symmetry of chip 2 was $+0.15$ mag, with an rms of 0.09 mag. (Unfortunately no similar grid of stars exists for the other chips, although we would expect comparable differences.) New empirical PSFs were then made for each chip, by combining the median images from the V30 and major axis fields (in order to have enough bright isolated stars in each chip). Systematic differences as a function of chip position are seen between these new and old empirical PSFs and the TinyTim PSFs. However, since we are calibrating the ALLFRAME mags directly against secondary standards in each of the fields (§§ 3 and 4), the zero-point differences were accounted for in the conversion of ALLFRAME mags ($F555W_{ALF}$ and $F785LP_{ALF}$) to standard mags (V and I), and the positional differences were less than the uncertainties in the secondary standard magnitudes. For example, the rms difference between the secondary standard mags and those derived from the old and new PSFs changed from 0.07 to 0.05 (chip 1), and from 0.14 to 0.10 (chip 2) in F555W, and from 0.14 to 0.15 (chip 1), and from 0.15 to 0.12 (chip 2) in F785LP. Nevertheless, we are continuing with experiments to improve our models of the WFC PSF.

3. GROUND-BASED PHOTOMETRY

A variety of telescopes were used to obtain photometry of the M81 fields in order to verify our calibrations. *BVRI* observations from the Canada-France-Hawaii Telescope (CFHT) were obtained on 1988 January 19–21 of the then only known Cepheids V30 and V2 (Madore, Freedman, & Lee 1993; Freedman & Madore 1988). Lower S/N data were also obtained at the Palomar 1.5 m by M. G. Lee on 1992 June 26, which confirmed the CFHT calibration at a level of 0.03 mag at V and 0.01 mag at I. Further confirmation that the CFHT night was photometric and the calibration reliable is inferred from a

comparison of photometry of NGC 2403 obtained on the CFHT on the same night as the M81 frame, and on the Kitt Peak National Observatory (KPNO) 4 m on 1984 March 23 by Madore & Freedman, which agree to better than ± 0.02 mag for *BVR* and *I* (Freedman, Lee, & Madore 1993).

Unfortunately, the CFHT photometry covers only a little more than half the M81 V30 field, and none of the major axis field. This was remedied by observations with the Palomar 5 m on the nights of 1992 June 8 and 9, using the COSMIC camera at the prime focus, with Johnson *V* and Gunn *i* filters (Fig. 1*a*, *b*). COSMIC was built by the Carnegie Observatories, and has a 2048 × 2048 Tektronix CCD with a gain of 3.8 electrons per ADU, a readout noise of 6.6 ADU, and a field of view of 9.5[2] Table 2 lists the M81 and standard fields observed, plus their exposure time (s), universal time, and airmass. All frames were bias-subtracted and divided by flat fields. For the *V* exposures, the flat fields for each night were obtained from a median of several twilight sky exposures. However, for the *i* flat field of June 8, only one twilight sky was obtained. This was used to characterize the general field variations due to vignetting, etc, by fitting a spline surface (with three knots). The pixel-to-pixel variations were obtained from a median of several dome exposures. To remove unwanted variations due to nonuniform dome illustration, this median dome image was divided by a spline-fitted surface. The real surface variations in the *i* flat were then restored by multiplying this by the surface fitted to the twilight flat.

Photometric data of the stellar images were determined from both synthetic aperture and PSF-fitting photometry, using DAOPHOT (Stetson 1987) and ALLSTAR (a second-generation profile-fitting algorithm which simultaneously fits overlapping profiles to all stars contained within a CCD image). Samples of the stellar PSF were obtained from ~20 to 50 visually isolated stars in each exposure (to allow for seeing variations between exposures). The aperture magnitudes as a function of aperture radius were inspected for each PSF star, and those that were markedly discrepant were discarded (as they were probable merged stars, H II regions, clusters, or background galaxies). Total magnitudes for the PSF stars were determined by fitting growth curves (using DAOGROW—Stetson 1990) to the aperture photometry, where aperture radii ranged from 2 to 20 pixels. The mean differences between these total magnitudes and the ALLSTAR (PSF) magnitudes were used to correct the ALLSTAR photometry of all stellar images to total magnitudes.

These ALLSTAR-derived total magnitudes ($v_{\rm tot}$ and $i_{\rm tot}$) were then corrected for atmospheric extinction (a function of airmass X) and varying exposure times (τ), as

$$v' = v_{\rm tot} - k_v X + 2.5 \log \tau_v , \quad \text{where } k_v = 0.26 ,$$
$$i' = i_{\rm tot} - k_i X + 2.5 \log \tau_i , \quad \text{where } k_i = 0.16 .$$

(Due to the eruption of Mount Pinatubo on 1991 June 15, the atmospheric extinction was higher than usual. The *k* extinction corrections were determined by M. G. Lee from Palomar 1.5 m photometry during 1992 June 21–25. The standard Palomar values are $k_v = 0.14$ and $k_i = 0.06$.)

Transformations to the standard Johnson *V* and Kron-Cousins *I* systems were made by least-squares fits to $v' - V$ and $V - I$ versus $v' - i'$, using the published *V* and *I* magnitudes in the Table 2 references (see Fig. 2). Observations at Palomar with the Gunn *i* filter are routinely transformed to the Cousins system, and there is no color term except for the very reddest stars (Tinney 1993). The night of June 8, although appearing clear, was perhaps smoggy at the start, as the v' mags were observed to decrease by ~0.1 mag between each of the PG 1323, M92, and SA 110 exposures. The $v' - V$ transform was therefore derived from PG 1323, as it was taken immediately after the M81 fields (Table 2). However, having no *i* exposure for PG 1323, the $V - I$ transform was derived from M92 and SA 110. The night of June 9 seemed to be photometric, but the transforms were derived from only the PG 1323, PG 1633, and G67−23 fields, as the M92 magnitudes were discrepant.

The adopted transformations are

June 8: $v' - V = -0.163(0.001) - 0.026(0.003)[v' - i']$,
$\sigma = 0.003$, $N = 3$;
$V - I = 0.390(0.003) + 1.009(0.002)[v' - i']$,
$\sigma = 0.056$, $N = 8$.

June 9: $v' - V = -0.367(0.002) - 0.035(0.003)[v' - i']$,
$\sigma = 0.011$, $N = 11$;
$V - I = 0.394(0.003) + 0.998(0.002)[v' - i']$,
$\sigma = 0.060$, $N = 11$.

The change in sensitivity between the two nights, as indicated by the ~0.2 mag difference in $v' - V$ zero points, is due to a different normalization used in the flat fields (corresponding to −0.07 mag from June 8 to June 9) and a decrease in sensitivity on the first night of 0.12 mag, due presumably to increased extinction (as determined from PG 1323—a standard field taken on both nights at an almost identical airmass). The accuracy of these transformations were confirmed by the CFHT photometry, which covered a portion of the V30 field. From the eight secondary standards in common between the COSMIC (Palomar 5 m) and CFHT frames (see Table 4), the mean difference in their photometry (COSMIC − CFHT) was $+0.05 \pm 0.03$ mag in *V*, -0.01 ± 0.03 mag in *I*, and $+0.06 \pm 0.03$ mag in $V - I$. This agreement is reflected in Figure 3, which shows the scatter in *V* and in *I* for all the stars in the CFHT/COSMIC V30 overlap which have ALLSTAR uncertainties less than 0.1 mag. Although there appears to be a slight discrepancy of ~0.1 mag for $21 < V < 22$, this is probably a statistical fluctuation, as the removal of the secondary

TABLE 2

PALOMAR 5 METER OBSERVATIONS

Field	*V* exposures			*i* exposures		
	Exp	UT	Airmass	Exp	UT	Airmass
		— 1992 June 8 —				
M81 major axis	182	4:14	1.45	180	4:20	1.48
M81 V30 field	180	4:36	1.51	180	4:30	1.49
PG1323[a]	20	5:07	1.40	...	...	...
M92[b]	20	6:42	1.05	20	6:28	1.06
SA110[a]	3	11:55	1.54	3	11:52	1.49
		— 1992 June 9 —				
PG1323[a]	5	3:50	1.35	5	3:56	1.35
M81 major axis	180	4:20	1.48	180	4:34	1.51
M92[b]	20	4:56	1.23	20	5:00	1.22
PG1633[a]	5	7:57	1.11	5	7:52	1.10
G67-23[c]	5	11:46	1.10	5	11:43	1.11

[a] Landolt 1992.
[b] Christian et al. 1985.
[c] Mould, Kristian, & Da Costa 1983.

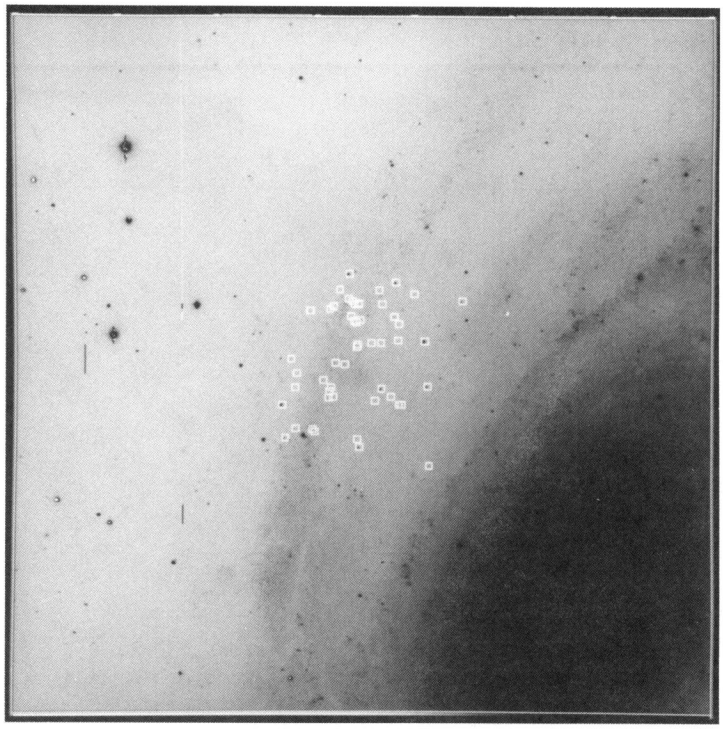

FIG. 1*a*

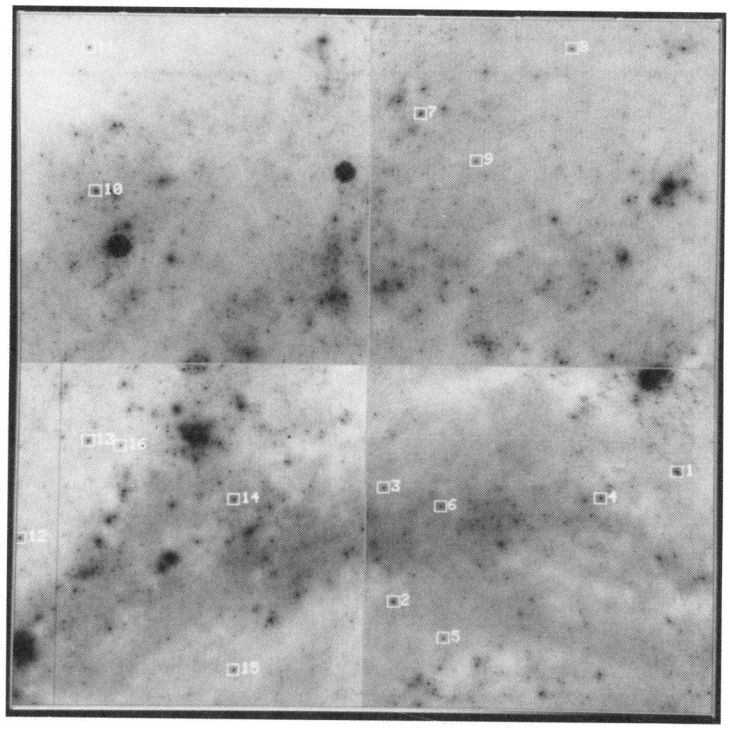

FIG. 1*b*

FIG. 1.—Full 2048 × 2048 COSMIC *V* image of the (*a*) V30 and (*b*) major axis fields in M81. The squares are the positions of the secondary standards. Corresponding mosaiced images of *HST* F555W median frames are given for the V30 (*c*) and major axis (*d*) fields, with the same standards identified as in (*a*) and (*b*), and numbered according to Table 4. The V30 field COSMIC image has north up, east to the left, with the *HST* image rotated 12° north toward east, and the major axis fields are rotated by 29° (COSMIC) and 41° (*HST*) north toward east.

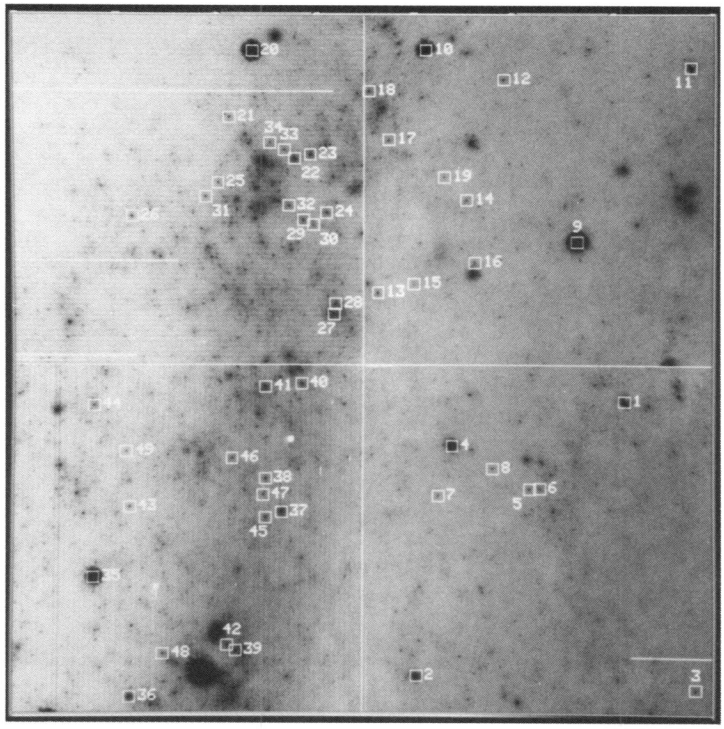

FIG. 1*c*

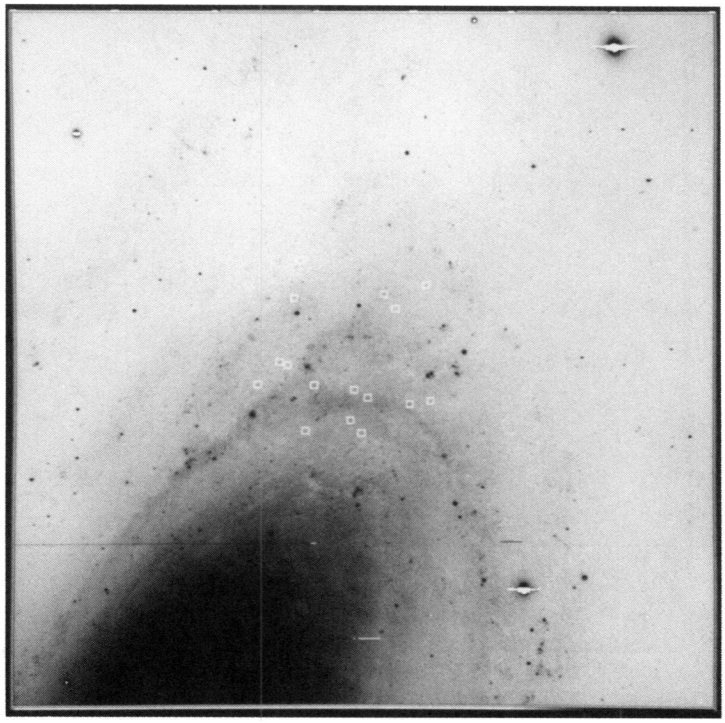

FIG. 1*d*

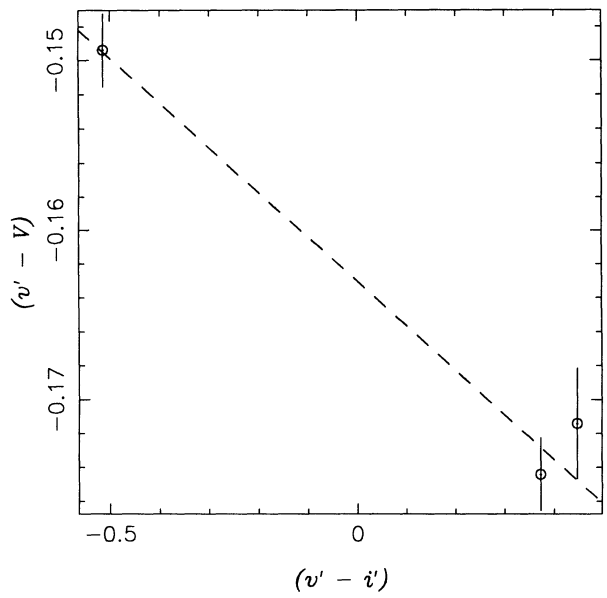

FIG. 2*a*

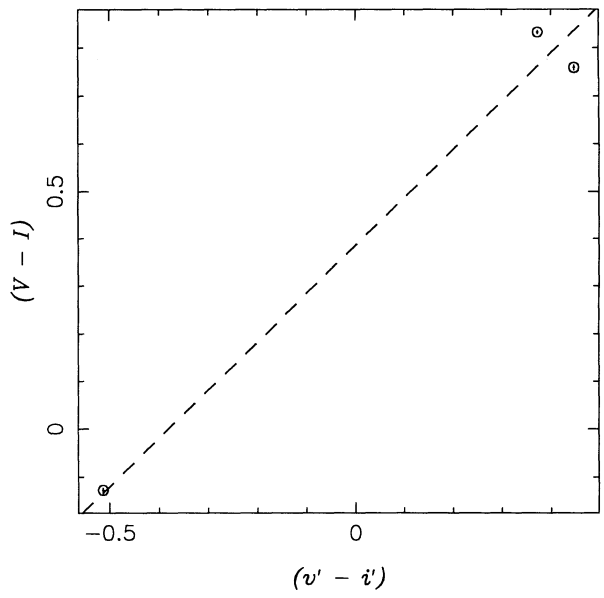

FIG. 2*b*

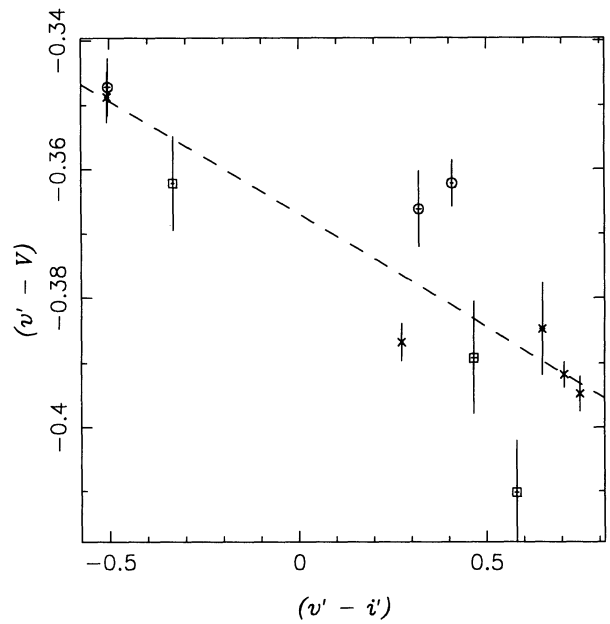

FIG. 2*c*

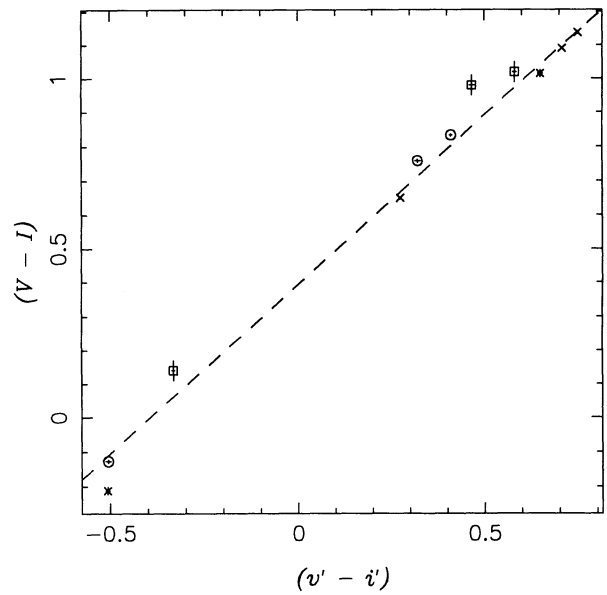

FIG. 2*d*

FIG. 2.—$v' - V$ and $V - I$ vs. $v' - i'$ for the standards observed with Palomar 5 m plus COSMIC camera, on 1992 June 8 (*a*, *b*) and 1992 June 9 (*c*, *d*). Circles are PG 1323 standards (−086, C and B), crosses are PG 1633 standards (A, B, C, D, and +0.99), and squares are G67−23 standards (−23, −123, −223), as referred to in Table 2. The dashed lines are least-squares fits to these data, and are the transformations used to convert the COSMIC photometry to standard (see text).

standards with $V > 21$ mag has no systematic effect on our final calibration. Confirmation of the accuracy of the major axis field (COSMIC) photometry is obtained from the large areas of overlap between the COSMIC (v30) and CFHT exposures, and the COSMIC major axis field exposures of June 8 and 9 (maj_8 and maj_9). The mean differences of the photometry of stars in the various overlap regions with $V < 21$ and $I < 20$ magnitudes (and ALLSTAR uncertainties less than 0.1 mag) are given in Table 3. We find that for V, all the ground-based photometry sets agree to better than 0.05 mag. However, the scatter in I shows that the major axis field COSMIC photometry of June 9 is of dubious quality.

4. CALIBRATION OF WFC PHOTOMETRY

Secondary standards in each of the *HST* WFC fields in M81 were established from the CFHT and COSMIC (PAL) photometry. These are listed in Table 4, which gives their identifying number corresponding to Figure 1*c*–*d*, their V and $V - I$ magnitudes (from the June 9 COSMIC photometry for the major axis), their mean ALLFRAME magnitudes, their positions with respect to the raw (800 × 800 pixels) *HST* frames, and their ALLFRAME identifier. The median *HST* WFC images were used to visually inspect each potential secondary standard, to ensure they were isolated stellar images (over half the

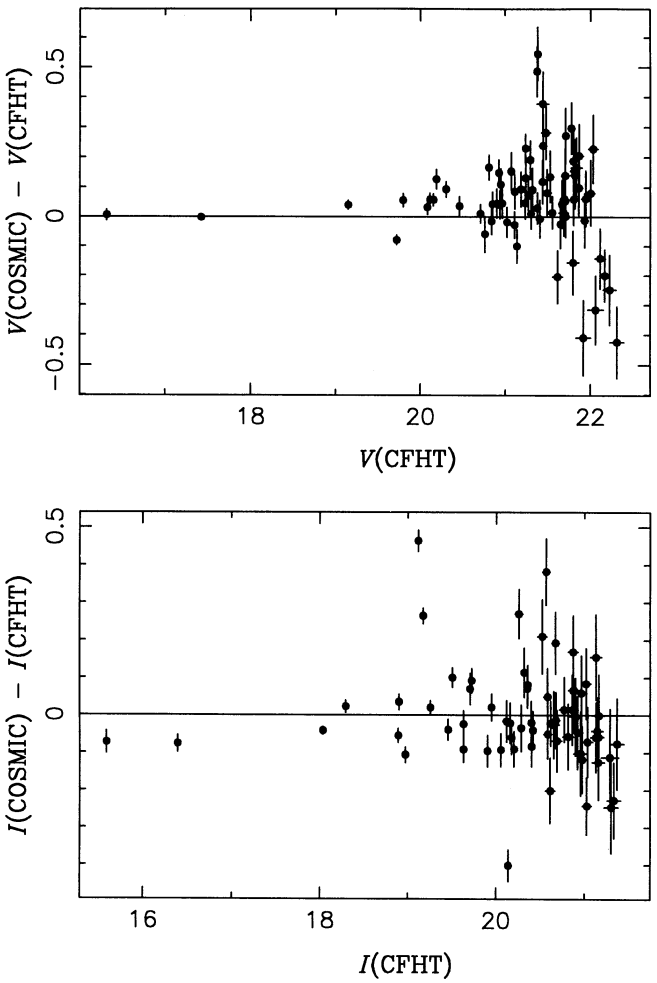

FIG. 3.—The difference in V (*upper panel*) and I (*lower panel*) magnitudes derived from independent exposures, for stars with ALLSTAR uncertainties less than 0.1 mag in the overlap region between the Palomar 5 m (COSMIC) V30 field taken on 1992 June 8, and the CFHT field taken on 1988 Jan 20.

"stellar images" identified on the COSMIC frames turned out to be H II regions or clusters on the *HST* frames).

For the 65 secondary standards selected, the F555W–F785LP colors ranged from −0.22 to 2.36 mag with a mean color of 0.48 mag, and the colors of the 31 Cepheids ranged from 0.60 to 1.65 with a mean of 1.05 mag. This range in color for the Cepheids is equivalent to a difference in F555W − V ∼ 0.02 mag, the F785LP − I ∼ 0.14 mag (Harris et al. 1991). We therefore ignored the color term in converting F555W mags to Johnson V. The large color term between F785LP and Kron-Cousins I can be accounted for by inverting the F785LP to I transform given in Harris et al. (1991), assuming $V-I$ = F555W − I.

TABLE 3

COMPARISON OF "OVERLAP" MAGNITUDES

Fields	V < 21 mag			I < 20 mag		
	N	ΔV	rms	N	ΔI	rms
(v30) −(CFHT)	21	0.05	0.06	18	0.03	0.14
(v30) −(maj_8)	133	0.02	0.12	119	0.03	0.18
(v30) −(maj_9)	154	−0.03	0.13	109	−0.12	0.25
(maj_8) −(maj_9)	357	−0.02	0.15	228	−0.17	0.13

The zero points needed to be added to the WFC instrumental (ALLFRAME) magnitudes to convert them to standard magnitudes are given by the mean differences between the ground-based secondary standard magnitudes and the ALLFRAME WFC magnitudes, which are given in Table 5 for each of the V30 and major axis fields. (For the purposes of comparing zero points, we have avoided the large color term between F785LP and I by transforming the ground-based I magnitudes to F785LP, as per Harris et al.). As the COSMIC major axis photometry sets for June 8 and June 9 disagree in I (Table 3), we present the mean differences for both sets of COSMIC photometry for the major axis field. Despite the use of different PSFs (see above) between the V30 and major axis fields in the WFC photometry, Table 5 shows the V − $F555W_{ALF}$ differences to be within ∼0.1 mag of each other for each of the four chips. However, for F785LP − $F785LP_{ALF}$, there is a much greater scatter (up to 0.4 mags for chip 1), indicating the quoted uncertainties for F785LP magnitudes are underestimated. We experimented with various possible correction methods, including fitting a surface to the old empirical PSF and TinyTim PSF magnitude differences of synthetic stars generated by the new empirical PSF, and fitting surfaces to the F555W and F785LP flat-field corrections (Phillips et al. 1993), but none systematically reduced the field-to-field differences. Therefore we combine the three uncorrected results of Table 5, to give mean offsets between the standard and ALLFRAME photometry, given in Table 6. These results are comparable to what we can derive from the IDT Report (the numbers in parentheses in Table 6), wherein corrections have been applied for the WFC sensitivity at F555W on 1992 January 3 (∼same date as the first of our M81 epochs, to which all the ALLFRAME magnitudes are transformed) and the differences in sensitivity between WFC chips (IDT Report Table 12.13), as well as the aperture correction from ALLFRAME magnitudes to total (radius of 40 pixels), measured to be 1.60 mag. The zero points given in Table 1 of Paper I were based on the mean of the V30 and June 9 major axis fields, but here we have taken the mean of all the photometry sets. The values for the V − $F555W_{ALF}$ zero points in Table 6 are 0.01 mag smaller than those in Table 1 of Paper I, while the zero points for F785LP − $F785LP_{ALF}$ differ by +0.05, +0.01, −0.02, and −0.02 for each of chips 1 to 4, compared to Table 1 of Paper I. These changes are quite small, and as noted in Paper I, the final distance modulus to M81 has remained unchanged.

The completeness limit of the calibrated V ALLFRAME photometry was determined by the recovery of simulated stars. These were produced by ADDSTAR in DAOPHOT II, where 100 stars with random magnitudes between V = 24.0 and 26.0 mag were added at random positions to each of five copies of the median image of the V30 chip 1 field. These images were then processed in the same way as the real frames. In Figure 4, the fraction of recovered stars as a function of V magnitude shows we have a recovery rate ∼90% up to V = 25 mag, after which the recovery rate declines sharply, indicating this is the completeness limit for the degree of crowding typical of the M81 fields. The mean difference between the recovered magnitudes and their true magnitudes for the V < 25.0 mag stars is −0.004, with an rms dispersion of 0.18 mag.

5. THE STELLAR POPULATION IN M81

When combined, our WFC observations provide total exposures of 400 minutes in F555W and 180 minutes in F785LP. Although these observations were optimized for the detection

TABLE 4

M81 SECONDARY STANDARDS

ID	V	$V-I$	F555W$_{ALF}$	(F555W−F785LP)$_{ALF}$	X *(HST)*	Y	ID$_{ALF}$
			— V30 field —				
	Chip 1 - PAL						
1	19.505 ± 0.012	1.063 ± 0.018	16.129 ± 0.028	0.643 ± 0.053	104.8	607.4	3569
2	19.641 ± 0.013	0.774 ± 0.021	13.352 ± 0.028	0.266 ± 0.056	703.7	156.0	759
3	21.705 ± 0.054	2.098 ± 0.063	18.404 ± 0.032	1.878 ± 0.076	728.5	758.5	4702
4	19.192 ± 0.013	1.198 ± 0.015	15.644 ± 0.037	0.394 ± 0.061	203.4	233.8	11183
	Chip 1 - CFHT						
5	22.180 ± 0.060	0.260 ± 0.250	18.752 ± 0.040	-0.876 ± 0.102	296.1	403.5	2134
6	22.214 ± 0.060	0.613 ± 0.115	18.830 ± 0.032	-0.476 ± 0.083	294.6	425.7	2278
7	22.309 ± 0.103	0.222 ± 0.141	18.897 ± 0.034	-1.084 ± 0.095	310.8	203.7	1020
8	22.643 ± 0.068	0.430 ± 0.305	19.151 ± 0.038	-1.645 ± 0.169	252.0	322.8	1698
	Chip 2 - PAL						
9	16.596 ± 0.011	0.856 ± 0.059	13.302 ± 0.145	-0.036 ± 0.389	493.6	300.7	1719
10	18.200 ± 0.005	1.000 ± 0.012	14.400 ± 0.051	0.167 ± 0.110	161.7	717.6	5213
11	20.139 ± 0.014	0.944 ± 0.022	16.633 ± 0.031	0.247 ± 0.059	733.0	678.5	11965
12	22.103 ± 0.089	0.454 ± 0.159	18.573 ± 0.035	-0.855 ± 0.102	331.6	652.9	4563
	Chip 2 - CFHT						
13	21.968 ± 0.234	0.385 ± 0.271	18.237 ± 0.080	-0.573 ± 0.170	58.4	191.8	1010
14	22.318 ± 0.119	0.233 ± 0.253	18.896 ± 0.038	-0.878 ± 0.119	252.9	390.3	12338
15	22.881 ± 0.019	0.749 ± 0.045	19.220 ± 0.041	-0.090 ± 0.099	137.2	210.2	433
16	22.696 ± 0.132	0.442 ± 0.182	19.080 ± 0.080	0.370 ± 0.170	271.6	256.6	11417
17	22.050 ± 0.045	0.094 ± 0.100	18.350 ± 0.034	-0.687 ± 0.091	81.4	519.9	3359
18	22.042 ± 0.114	0.001 ± 0.140	18.175 ± 0.080	-0.908 ± 0.170	36.7	626.7	1750
19	22.872 ± 0.084	0.376 ± 0.147	19.222 ± 0.044	-0.969 ± 0.134	203.2	439.6	2721
	Chip 3 - PAL						
20	17.316 ± 0.005	0.979 ± 0.017	13.471 ± 0.061	0.084 ± 0.091	703.7	283.3	1
21	21.894 ± 0.069	2.047 ± 0.073	18.136 ± 0.029	1.467 ± 0.058	558.4	333.8	55
22	20.303 ± 0.021	1.048 ± 0.030	16.587 ± 0.026	0.310 ± 0.050	468.2	191.2	6
23	20.689 ± 0.024	0.258 ± 0.053	17.001 ± 0.027	-0.634 ± 0.063	477.2	156.3	12
24	21.514 ± 0.065	0.306 ± 0.110	17.962 ± 0.027	-0.665 ± 0.059	352.0	119.7	46
25	21.916 ± 0.072	0.103 ± 0.172	18.228 ± 0.029	-0.689 ± 0.083	416.1	358.2	68
26	22.068 ± 0.072	0.696 ± 0.118	18.490 ± 0.035	-0.340 ± 0.080	343.2	542.5	71
	Chip 3 - CFHT						
22	20.250 ± 0.058	0.994 ± 0.054	16.587 ± 0.026	0.310 ± 0.050	468.2	191.2	6
23	20.707 ± 0.024	0.214 ± 0.042	17.001 ± 0.027	-0.634 ± 0.063	477.2	156.3	12
24	21.362 ± 0.030	0.260 ± 0.085	17.962 ± 0.027	-0.665 ± 0.059	352.0	119.7	46
25	21.998 ± 0.074	0.239 ± 0.159	18.228 ± 0.029	-0.689 ± 0.083	416.1	358.2	68
26	21.905 ± 0.044	0.563 ± 0.075	18.490 ± 0.035	-0.340 ± 0.080	343.2	542.5	71
27	20.343 ± 0.012	-0.155 ± 0.044	16.737 ± 0.028	-0.947 ± 0.061	134.5	103.5	9
28	21.268 ± 0.091	-0.011 ± 0.120	17.510 ± 0.028	-0.914 ± 0.063	156.4	99.7	30
29	21.297 ± 0.062	0.197 ± 0.299	17.704 ± 0.028	-0.571 ± 0.072	336.3	171.3	36
30	22.161 ± 0.046	0.217 ± 0.190	18.633 ± 0.031	-0.926 ± 0.074	325.5	149.5	95
31	21.686 ± 0.090	0.234 ± 0.108	17.967 ± 0.027	-0.654 ± 0.071	386.0	385.0	50
32	21.778 ± 0.034	0.014 ± 0.172	18.101 ± 0.029	-0.782 ± 0.068	366.9	203.5	53
33	22.350 ± 0.070	0.601 ± 0.087	18.674 ± 0.032	-0.606 ± 0.066	487.6	213.2	115
34	22.144 ± 0.064	0.190 ± 0.163	18.786 ± 0.033	-0.387 ± 0.073	502.5	245.6	121
	Chip 4 - PAL						
35	17.421 ± 0.005	1.103 ± 0.021	13.881 ± 0.040	0.897 ± 0.076	611.5	499.4	8744
36	20.116 ± 0.019	0.576 ± 0.031	16.530 ± 0.027	-0.112 ± 0.051	532.0	760.1	26
37	20.173 ± 0.019	0.756 ± 0.029	16.602 ± 0.027	0.054 ± 0.051	205.8	358.6	28
38	21.625 ± 0.072	0.140 ± 0.135	18.031 ± 0.028	-0.673 ± 0.068	241.8	285.5	90
	Chip 4 - CFHT						
36	20.081 ± 0.060	0.455 ± 0.060	16.530 ± 0.027	-0.112 ± 0.051	532.0	760.1	26
37	20.113 ± 0.015	0.664 ± 0.070	16.602 ± 0.027	0.054 ± 0.051	205.8	358.6	28
38	21.626 ± 0.067	0.033 ± 0.181	18.031 ± 0.028	-0.673 ± 0.068	241.8	285.5	90
39	20.966 ± 0.033	0.353 ± 0.062	17.616 ± 0.032	-0.064 ± 0.054	304.2	659.9	61
40	21.103 ± 0.058	0.161 ± 0.157	17.682 ± 0.028	-0.721 ± 0.065	163.4	79.2	50
41	20.874 ± 0.066	0.467 ± 0.098	17.906 ± 0.037	0.031 ± 0.070	242.8	85.2	54
42	21.480 ± 0.053	0.326 ± 0.091	18.011 ± 0.029	-0.533 ± 0.059	322.5	647.3	95
43	21.887 ± 0.047	0.201 ± 0.160	18.087 ± 0.031	-0.642 ± 0.070	534.8	346.4	112
44	21.473 ± 0.052	0.297 ± 0.064	18.131 ± 0.029	-0.368 ± 0.065	613.1	126.1	79
45	21.691 ± 0.003	0.205 ± 0.251	18.290 ± 0.030	-0.380 ± 0.064	241.2	369.6	115
46	22.007 ± 0.098	-0.044 ± 0.124	18.330 ± 0.028	-0.631 ± 0.056	314.9	241.8	114
47	21.954 ± 0.053	0.017 ± 0.183	18.332 ± 0.028	-0.925 ± 0.066	246.5	320.1	118
48	21.829 ± 0.070	0.175 ± 0.137	18.375 ± 0.029	-0.739 ± 0.067	461.1	665.8	127
49	22.115 ± 0.022	1.115 ± 0.073	18.408 ± 0.031	0.431 ± 0.052	542.5	226.2	140

TABLE 4 — *continued*

ID	V	$V-I$	F555W$_{ALF}$	(F555W−F785LP)$_{ALF}$	X (*HST*)	Y	ID$_{ALF}$
			— Major axis field —				
	Chip 1 - PAL						
1	20.224 ± 0.023	0.759 ± 0.035	16.651 ± 0.012	0.105 ± 0.027	253.6	714.6	2271
2	20.984 ± 0.045	0.478 ± 0.069	17.503 ± 0.008	-0.544 ± 0.031	551.9	101.9	218
3	21.206 ± 0.067	-0.211 ± 0.139	17.690 ± 0.015	-0.336 ± 0.035	299.3	77.1	140
4	21.115 ± 0.058	0.129 ± 0.086	17.706 ± 0.012	-0.661 ± 0.029	315.2	551.4	1702
5	21.720 ± 0.082	0.037 ± 0.155	17.930 ± 0.010	-0.962 ± 0.042	630.1	213.0	610
6	21.606 ± 0.089	0.316 ± 0.141	18.336 ± 0.016	-0.204 ± 0.040	339.3	203.5	578
	Chip 2 - PAL						
7	20.685 ± 0.032	0.164 ± 0.064	16.798 ± 0.012	-0.636 ± 0.026	136.8	582.4	3406
8	21.216 ± 0.041	0.214 ± 0.084	17.792 ± 0.014	-0.642 ± 0.033	465.4	729.2	4277
9	21.564 ± 0.072	0.212 ± 0.118	17.999 ± 0.014	-0.454 ± 0.033	261.1	480.1	2808
	Chip 3 - PAL						
10	20.323 ± 0.025	-0.122 ± 0.055	16.856 ± 0.016	-0.719 ± 0.030	395.1	633.1	4546
11	21.429 ± 0.053	0.212 ± 0.091	17.675 ± 0.018	-1.347 ± 0.054	709.0	645.9	4626
	Chip 4 - PAL						
12	20.855 ± 0.042	0.084 ± 0.076	17.079 ± 0.016	-1.155 ± 0.044	773.4	426.3	2860
13	20.937 ± 0.046	0.152 ± 0.082	17.203 ± 0.016	-0.651 ± 0.032	633.4	209.9	1084
14	21.166 ± 0.055	-0.092 ± 0.109	17.655 ± 0.017	-0.687 ± 0.038	316.9	339.1	2053
15	21.230 ± 0.058	1.454 ± 0.062	17.680 ± 0.016	0.815 ± 0.042	311.6	714.7	5758
16	22.019 ± 0.096	0.417 ± 0.146	18.383 ± 0.018	-0.337 ± 0.044	564.6	220.2	1150

TABLE 5

CALIBRATION OF WFC PHOTOMETRY

Chip	N	V−F555W$_{ALF}$	F785LP−F785LP$_{ALF}$
		— V30 field —	
1	8	3.40 ± 0.03	2.38 ± 0.17
2	11	3.62 ± 0.05	2.69 ± 0.12
3	15	3.64 ± 0.03	2.73 ± 0.04
4	15	3.51 ± 0.04	2.81 ± 0.05
		— Major axis field (June 8) —	
1	6	3.39 ± 0.03	2.76 ± 0.22
2	3	3.57 ± 0.07	2.74 ± 0.18
3	2	3.50 ± 0.10	2.42 ± 0.33
4	5	3.50 ± 0.08	2.64 ± 0.09
		— Major axis field (June 9) —	
1	6	3.51 ± 0.07	2.80 ± 0.14
2	3	3.63 ± 0.14	2.84 ± 0.15
3	2	3.61 ± 0.14	2.53 ± 0.35
4	5	3.64 ± 0.05	2.80 ± 0.07

TABLE 6

CALIBRATION OF MEAN WFC PHOTOMETRY

Chip	N	V − F555W$_{ALF}$		F785LP − F785LP$_{ALF}$	
		Ground-based	IDT Report	Ground-based	IDT Report
1	18	3.44 ± 0.03	(3.51)	2.61 ± 0.11	(2.70)
2	17	3.61 ± 0.04	(3.68)	2.73 ± 0.08	(2.73)
3	19	3.62 ± 0.03	(3.66)	2.69 ± 0.05	(2.59)
4	25	3.53 ± 0.04	(3.57)	2.78 ± 0.04	(2.61)

and measurement of Cepheid variable stars, these data also allow us to study the properties of the M81 stellar population in general. In this section we discuss the stellar luminosity functions and color-magnitude diagrams in the major axis and V30 fields.

We used the ALLFRAME photometry to compute weighted average magnitudes for each star and an rms dispersion about the mean magnitude. There were some faint stars that were visible on the median images that were not included in the ALLFRAME input list, but their photometric errors are too large to be useful here. The total number of "stars" detected in all the F555W frames was 42,061. In an attempt to remove any spurious detections, we selected only those stars that appeared in at least 12 of the 14 long-exposure (1200 s) F555W frames. As well, the stars were sorted by magnitude into 0.25 mag width bins, and the rms dispersions about the mean magnitudes of each bin were computed. We then removed those stars whose individual rms dispersion was more than 3 times the standard deviation for stars in that magnitude bin, as these are likely to be either variable stars or have been contaminated by cosmic-ray hits. This left us with 28,088 stars from both fields, which were used to produce the luminosity function (LF) in Figure 5. The turnover at $V \sim 25$ mag agrees with the completeness limit determined from the recovery of artificial stars (Fig. 4). The limiting magnitude for these combined exposures, defined by the faintest stars measured, is at $V \sim 27.0$ mag, although it is debatable how meaningful such a figure is, given

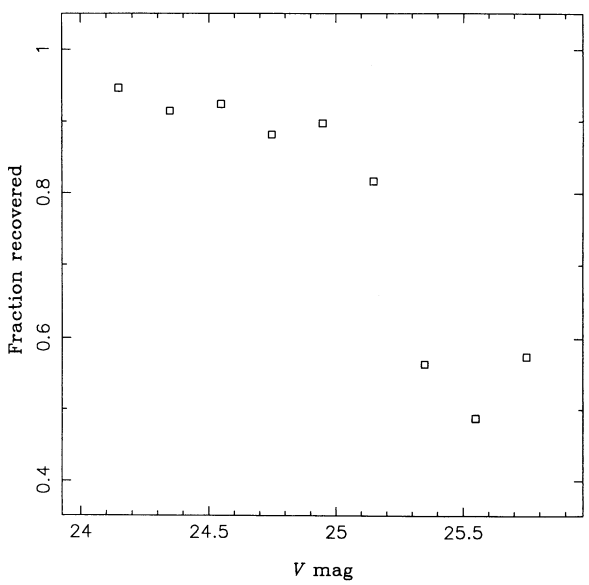

FIG. 4.—The fraction of artificial stars recovered from a median image of the V30 chip 1 field. Each of the 0.2 mag bins had ~50 artificial stars.

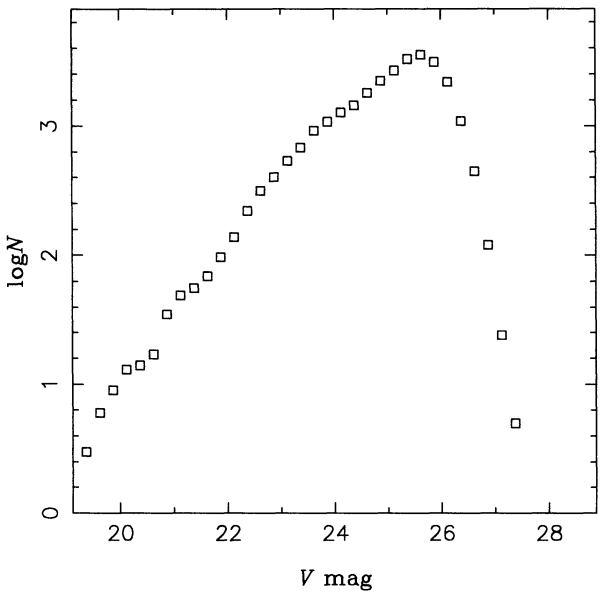

FIG. 5.—Calibrated V luminosity function of stars that were recovered in at least 12 of the 14 long-exposure (1200 s) F555W epochs in all chips and in both M81 fields, and which had rms dispersions about their mean of less than 3 standard deviations (as these are likely to have been severely contaminated by cosmic-ray hits).

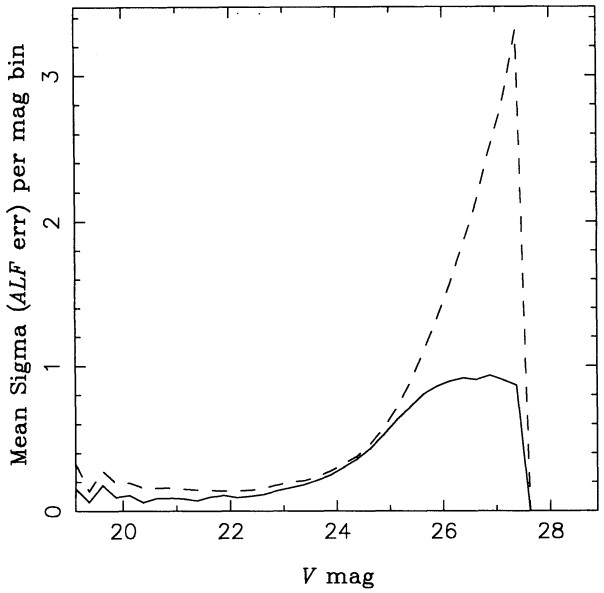

FIG. 6.—The solid line is the mean rms dispersion about the mean of the 12–14 epoch magnitudes of the stars in Fig. 5, for each of 40 magnitude bins. The dashed line is the mean single-epoch uncertainty given by ALLFRAME in the same magnitude bins.

that the uncertainties at this level are ~ 1 mag. However, this is comparable to the limiting magnitude obtained by Holtzman et al. (1991), who reached $V \sim 24.5$ for an 1800 s F555W exposure of NGC 925: the equivalent exposure time for our deepest median images is $\sim 16{,}000$ s, implying we would reach $V \sim 24.6$ in 1800 s.[5]

The rms uncertainties in the magnitudes of the stars that form the total LF (Fig. 5) are shown in Figure 6, which plots the mean rms dispersion from the 12–14 F555W long-exposure epochs about the mean magnitude in each of 40 magnitude bins (*solid line*). Also plotted (*dashed line*) are the mean single-epoch uncertainties for each magnitude, as calculated by ALLFRAME. Consistent agreement is seen down to $V \leq 25$ mag, beyond which the ALLFRAME uncertainties and rms dispersions start to lose meaning, as they are for magnitudes clearly beyond the limit of our exposures. For the 377 bright stars with $V < 22$ mag, the mean rms dispersion is 0.09 mag (and ranges from 0.06 to 0.18 mag), compared to a mean ALLFRAME uncertainty of 0.16 mag.

For the purpose of comparing M81 with stellar populations in other galaxies, we also derived LFs with red stars ($V-I > 0.24$ mag) excluded. These LFs are shown in Figure 7. In this case the V LFs show a turnover at roughly a magnitude brighter than in Figure 5, which is mainly due to the shallower detection limit in F785LP (the LF in Fig. 5 was derived from stars with F555W magnitudes, regardless of whether or not they also had an F785LP magnitude). The slopes of the LFs lie in the range 0.56–0.58 mag^{-1}, where the slope (s) is defined as $s = d \log N(V)/dV$, for $V < 23.5$ mag. These values are consistent with those derived by Zickgraf & Humphreys (1991) (0.51 ± 0.08 mag^{-1} for $19 \leq V < 21$ mag and $B-V \leq 0.4$

[5] There is no exact correspondence between the total exposure time of all the images and the resultant median image from which the stars were detected, but as an approximation, we have assumed the equivalent exposure time is two-thirds the total exposure time.

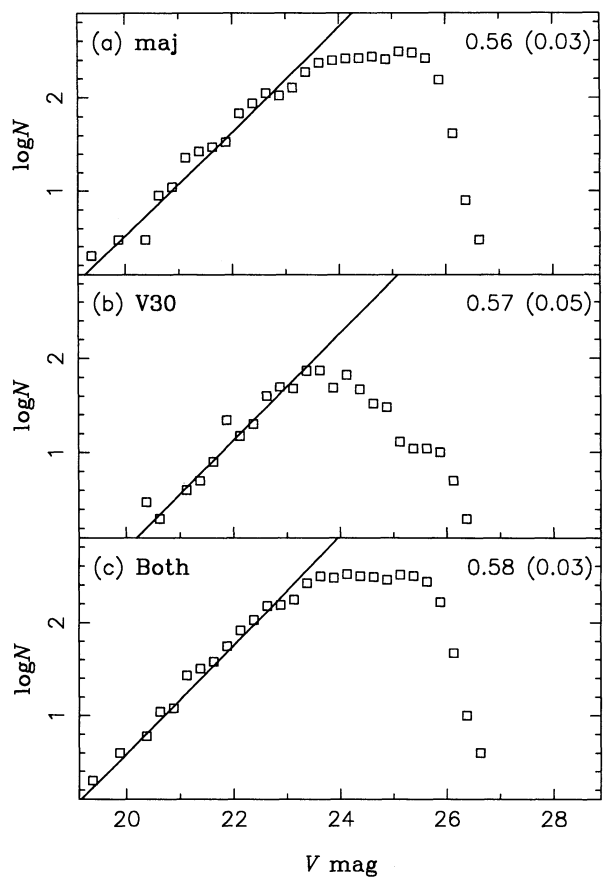

FIG. 7.—V luminosity functions for stars with $V-I < 0.24$ mag. The fit to the bright end is plotted as a line. The slope is given in upper right corner of each panel with uncertainty in fit given in parentheses. Panels show data for (*a*) major axis, (*b*) V30, and (*c*) both fields.

TABLE 7

COMPARATIVE V PHOTOMETRY

Star[a]	V(S84)[a]	V(ZH91)[b]	V(This Paper)	Field	Chip	X (*HST*)	Y	ID_{ALF}	Comments
37	20.20	20.17	20.13	V30	4	205.8	358.6	28	
38	20.30	20.00	20.06	V30	4	532.0	760.1	26	
139	20.00	...	19.95	maj	3	251.4	472.9	3434	
R155	20.83	20.92	20.74	maj	2	142.3	637.0	3746	
607[b]	...	19.88	19.79	V30	1	703.8	156.0	759	
140	20.50	...	20.48	maj	3	395.1	633.1	4546	
R36	20.45	...	20.31	V30	3	45.3	204.2	10	possible small cluster
R156	20.40	20.56	21.78	maj	2	95.3	211.3	1053	non-stellar profile
R1258[b]	...	20.66	21.32	maj	4	606.5	432.8	2924	2 companions within 1″

[a] Sandage 1984; [b] Zickgraf & Humphreys 1991

mag) and Madore et al. (1994) from ground-based measurements at brighter magnitudes. Our values are also similar to those measured for other nearby late-type galaxies by Freedman (1985).

Previously published photometry of the brightest blue and red stars in M81 are given in Sandage (1984) and Zickgraf & Humphreys (1991). Our fields contain nine of these stars. A comparison of the V photometry is given in Table 7. Six of the objects appear as single stars in our frames, and for these the respective magnitudes agree well to within their respective uncertainties. However, two of the stars show companions within 1″ radius, and a third star (R156) is clearly extended on our WFC frames. In two of these cases we measure a fainter magnitude for the (central) star, as expected. It is impossible to draw any firm conclusions from a sample of only nine stars, but it is sobering to note that the ground-based photometry for two of the nine stars, all red supergiants, is seriously affected by crowding. If this is typical it would severely limit the accuracy of these stars as distance indicators in more distant galaxies, even when measured with *HST*.

Figure 8 shows the I versus $V-I$ color-magnitude diagrams (CMDs) for the major axis and V30 fields. As the mean reddening for these fields, relative to the LMC, is estimated to be only $E(B-V) = 0.03$ mag (Paper I), no reddening corrections have been applied. The CMDs in both fields are similar, which is expected as both regions seem to be of similar chemical composition,[6] and are dominated by supergiants. A comparison of the observed number counts with published Bahcall-Soneira models (Bahcall & Soneira 1981; Ratnatunga & Bahcall 1985) shows that any contamination by Milky Way field stars should be negligible.

In Figure 9 we plot the combined CMD for both fields, and overplot the expected loci for the upper main sequence, red supergiants, and red disk giants. These loci were taken from the I versus $V-I$ CMD of Shapley Constellation III in the LMC measured by Reid, Mould, & Thompson (1987). The right side of Figure 9 shows the absolute magnitude scale, derived using the distance modulus of 27.80 mag from Paper I. The M81 fields show the characteristic broad "blue plume" that is observed in other external galaxies (e.g., Freedman 1985), and the plume aligns nicely with the main-sequence locus in Shapley III. The color spread observed in M81 is probably due to a combination of photometric errors and variable reddening across the field. Numerous red supergiants are also observed, with the upper limit corresponding roughly to those in the LMC Shapley III field. The CMDs of the M81 fields are also very similar to that measured for the disk of M33 from ground-based measurements (Wilson, Freedman, & Madore 1990). This similarity in CMD morphologies is not surprising, as both galaxies contain an abundance of H II regions and young star-forming regions, which dominate the CMD in this luminosity range. Inspection of the images shows that the brightest supergiants are concentrated along the spiral arms and in OB/H II association complexes, and this is confirmed by individual CMDs obtained for several selected associations.

Of the 30 Cepheid variables reported in Paper I, 25 have reliable magnitudes in both V and I, and these are denoted by open triangles in Figure 9. As expected, the Cepheids occupy the instability strip in the CMD. Other variables identified in Figure 9 are two eclipsing binaries (*squares*) located in the blue plume, and several long-period variable (LPV) candidates (*circles*). The four LPV candidates with $V-I > 1.5$ mag are likely red supergiant LPVs, for which we would expect their periods to be between 100 and 900 days, as found for the LMC supergiant LPVs (Wood, Bessell, & Fox 1883). Since the *HST* data do not extend over a long enough baseline for us to measure such long periods, further (red) exposures of these fields are being taken in *HST* cycles 3 and 4. The blue faint LPV candidates, if not spurious, may turn out to be R CrB variables (which we should be able to verify with the cycle 3 and 4 data), and the one bright LPV candidate with $V-I \sim 1.0$ mag may be a long-period Cepheid. Unfortunately our data are not quite deep enough to study the underlying disk giant population in M81, as illustrated in Figure 9. Although giants are probably detected (especially in our stacked images), they lie too close to the magnitude limit of our data to be reliably measured.

Further interpretation of the CMDs will require WFC observations at a bluer bandpass (U and/or B), in order to constrain the reddening and provide better color discrimination of blue stars. Such observations are proposed for future *HST* cycles.

6. CONCLUSIONS

Using the calibration in Table 6, the mean V magnitudes of the Cepheids found in M81 ranged from 21.6 to 23.8 mag (and their periods ranged from 55 to 10 days), corresponding to single epoch magnitude uncertainties (Fig. 6) of 0.1–0.3 mag, respectively. The uncertainties from the multiepoch (22) magnitude sample should therefore be in the range 0.02–0.06 mag (but will depend on their position and environment, and how

[6] See Paper I for a discussion of the abundances in the two M81 fields. Based on published H II region observations, the mean abundances are $12 + \log(O/H) = 8.85$ for the major axis field and 8.65 for the V30 field.

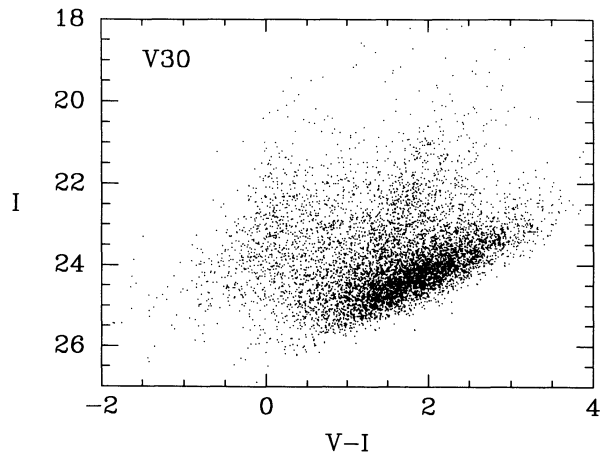

FIG. 4*a*

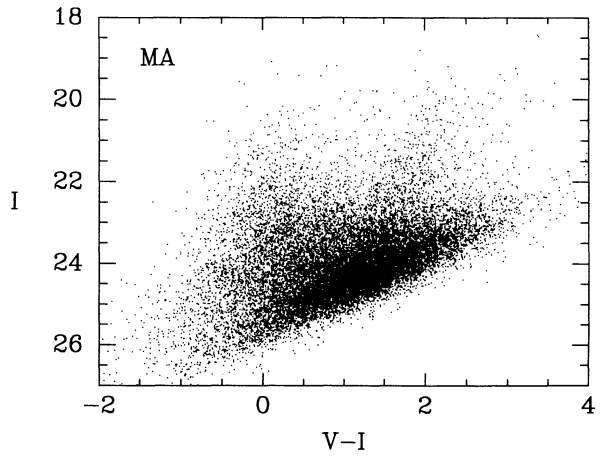

FIG. 4*b*

FIG. 8.—I vs. $V-I$ color magnitude diagrams for (*a*) the V30 and (*b*) the major axis fields. These contain 7129 and 18,953 stars, respectively.

well their light curve is sampled). Combining all 30 Cepheid magnitudes results in an uncertainty in the zero point of a line of best fit to the $P-L$ relation of 0.05 mag (Paper I). The CMD analysis shows that all the Cepheids are located in the instability strip, and that the stellar populations in these two M81 fields have similar magnitudes and colors as those in the disk of M33.

We are continuing to work on improved characterization of the WFC PSF. Alternative representations can be evaluated from the residuals from our fit to the secondary standards or indeed any WFC images of high S/N with suitably different telescope pointings. We find that within 300 pixels of chip centers PSFs derived from real and simulated stars yield magnitudes with rms differences of 0.06 mag. This covers just over half the effective field. Over the field as a whole we see rms differences up to 0.15 mag. Improved PSFs should lead to a reduction in these field effects, but given the large number of secondary standards we are employing, they are not expected to significantly change the zero point of our photometric calibration.

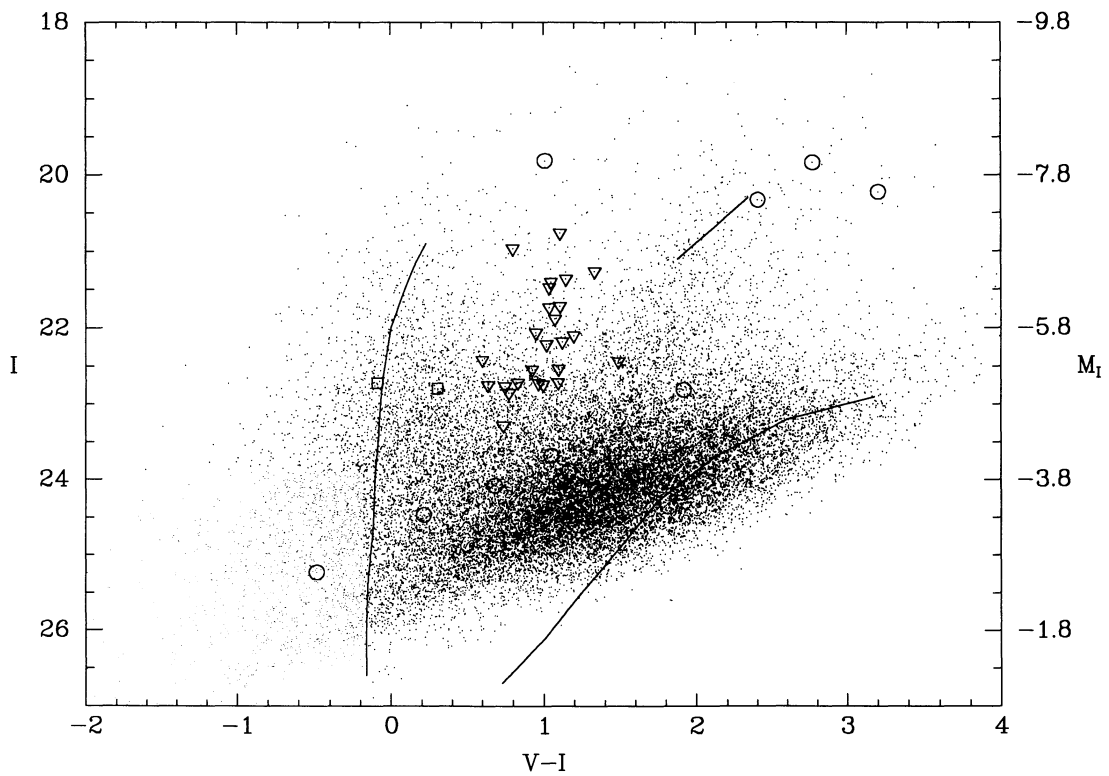

FIG. 9.—I vs. $V-I$ color magnitude diagram for all 26,082 stars detected in V and I in M81. Lines represent main sequence, red giant, and red supergiant loci from Shapley III in the LMC (Reid et al. 1987). Open triangles are Cepheids (see Paper I). Open squares are eclipsing variables, and open circles are long-period variable candidates. The absolute magnitude scale is shown on the right, based on a distance modulus of 27.80 mag to M81.

Support for this work was provided by NASA through grant number 2227-87A from the Space Telescope Science Institute which is operated by the Association of Universities for Research in Astronomy, Inc., under NASA contract NAS 5-26555. B. F. M. is supported in part by the NASA/IPAC Extragalactic Database (NED) and the Jet Propulsion Laboratory, Caltech. The ground-based calibration was supported in part by NSF grants AST-87-13889 and AST-91-16496 to W. L. F. We are grateful to Alan Dressler and Bill Kells of the Carnegie Observatories for their time and effort in building the excellent COSMIC camera used on the Palomar 5 m. We also thank the staff of the Palomar Observatory for their as usual splendid work of maintaining instruments and telescopes, and for their assistance during observing. We also thank the referee for the useful comments that have helped clarify the paper.

REFERENCES

Bahcall, J. N., & Soneira, R. M. 1981, ApJS, 47, 357
Burrows, C. J., et al. 1991, ApJ, 369, L21
Christian, C. A., Adams, M., Barnes, J. V., Butcher, H., Hayes, D. S., Mould, J. R., & Siegel, M. 1985, PASP, 97, 363
Faber, S. M., et al. 1991, WF/PC Orbital Science Verification Report, STScI
Freedman, W. L. 1985, ApJ, 299, 74
Freedman, W. L., Lee, M. G., & Madore, B. F. 1993, in preparation
Freedman, W. L., & Madore, B. F. 1988, ApJ, 332, L63
Freedman, W. L., et al. 1992, ApJ, 396, 80
———. 1994, ApJ, 427, 628 (Paper I)
Harris, H. C., Baum, W. A., Hunter, D. A., & Kreidl, T. L. 1991, AJ, 101, 677
Holtzman, J. A., et al. 1991, AJ, 369, L35
Hughes, S. M. G. 1992, in IAU Colloq. 136, Stellar Photometry, Current Techniques & Future Developments, ed. C. J. Butler & I. Elliott (Cambridge: Cambridge University Press), 352
Labhardt, L., Schwengeler, H., & Tammann, G. 1993, ST-ECF Newsletter 19, 13
Landolt, A. U. 1992, AJ, 104, 340
Lauer, T. R. 1989, PASP, 101, 445
Madore, B. F., Freedman, W. L., & Lee, M. G. 1994, AJ, in press
Mateo, M., & Schechter, P. 1989, in 1st ESO ST-ECF Data Analysis Workshop, ed. P. J. Grosbol, F. Murtagh, & R. H. Warmels (Garching: ESO), 69
Mould, J. R., Kristian, J., & Da Costa, G. S. 1983, ApJ, 270, 471
Mould, J. R., et al. 1993, BAAS, in press
Phillips, A. C., Forbes, D. A., Bershady, M. A., Illingworth, G. D., & Koo, D. C. 1993, AJ, in press
Ratnatunga, K. U., & Bahcall, J. N. 1985, ApJS, 59, 63
Reid, N., Mould, J., & Thompson, I. 1987, ApJ, 323, 433
Ritchie, C. E., & MacKenty, J. W. 1993, WF/PC Instrument Science Report 93-02, STScI
Sandage, A. R. 1984, AJ, 89, 621
Stetson, P. B. 1987, PASP, 99, 101
———. 1990, PASP, 102, 932
———. 1991, in Astronomical Data Analysis Software and Systems I (ed. D. M. Worrall, C. Biemesderfer, & J. Barnes (ASP Conf. Ser. 25), 297
———. 1992, in 3rd ESO/ST-ECF Data Analysis Workshop, ed. P. J. Grosbol & R. H. Warmels (ESO Conference and Workshop Proc. No. 38) (Garching: ESO), 187
———. 1994, in preparation
Tinney, C. G. 1993, Ph.D. thesis, California Institute of Technology
Wilson, C. D., Freedman, W. L., & Madore, B. F. 1990, AJ, 99, 149
Wood, P. R., Bessell, M. S., & Fox, M. W. 1983, ApJ, 272, 99
Zickgraf, F.-J., Humphreys, R. M. 1991, AJ, 102, 113